Predicting Polymer Flow during High-Temperature Atomic Force Microscope Nanoindentation

Harry D. Rowland and William P. King*

Department of Mechanical Science and Engineering, University of Illinois Urbana−Champaign, Urbana, Illinois 61801

Amy C. Sun and P. Randy Schunk

Dept. 1514, Multiphase Transport Processes, Sandia National Laboratories, Albuquerque, New Mexico 87185-0827

Graham L. W. Cross

SFI Trinity Nanoscience Laboratory, Trinity College, Dublin 2, Ireland

Received February 18, 2007; Revised Manuscript Received June 17, 2007

ABSTRACT: This paper reports predictions of nanometer-scale polymer deformation during nanoprobe indentation at elevated temperature. The simulations assume continuum polymer properties with modified boundary conditions to model subcontinuum polymer mechanical deformation. The indenter is a heated atomic force microscope (AFM) tip, and the media is a high molecular weight polymer film where tip radius, film thickness, and polymer coil radius are of similar size, in the range 20−50 nm. The simulations model isothermal conditions, where the tip and polymer are at the same temperature, or nonisothermal conditions, where the tip is hot while the polymer is cool. Isothermal simulations with shear-thinning bulk material behavior and full-slip polymer−tip interface predict force, displacement, and displacement rate. Nonisothermal simulations show that the polymer−tip interface temperature governs the indentation process. The temperature-dependent polymer viscosity varies by several orders of magnitude within 50 nm of the polymer−tip interface, causing highly localized polymer deformation near the tip. Steep viscosity gradients near the tip require the polymer−tip interface temperature to exceed the polymer glass transition temperature in order to form indents. In all cases the predictions compare well with experimental data. The continuum simulations allow for improved understanding of high-temperature AFM nanoindentation and nanoembossing.

Introduction

Embossing and molding are simple techniques for high fidelity replication. Recent studies have shown replication of single-walled carbon nanotubes with diameter 2 nm via molding[1] and crack tips of size 0.4 nm via casting.[2] Nanoimprint lithography (NIL)[3] offers scalable embossing or molding of sub-10 nm features over large areas.[4] One type of nanoembossing process with application to data storage is atomic force microscope (AFM) nanoindentation, shown in Figure 1, where a sharp conical tip forms indents into a thin polymer film.[5] This paper seeks to understand nanometer-scale polymer transport in isothermal and nonisothermal AFM nanoindentation with features as small as a few nanometers.

As polymer film thickness and indentation sizes shrink to 10 nm during nanoindent formation, the polymer thermomechanical behavior may deviate from that of bulk. The decrease in polymer film thickness increases surface to volume ratio and may confine the polymer molecules, resulting in increased influence of substrate interaction, stress history, and free surface properties on the glass transition temperature T_g and other modes of polymer mobility.[6,7] Confinement effects in thin polymer films have resulted in nonuniform T_g profiles across the film,[8,9] reduced temperature dependence on viscosity,[10] and suppressed particle diffusion.[11]

For data storage[5] and direct-write lithography,[12] an AFM tip embosses a thin polymer film that is constrained by a substrate. The polymer is typically a high molecular weight (M_W) thermoplastic. Figure 1 shows the AFM nanoindentation process, where the polymer deformation is localized to the region near the tip. The key length scales in these nanometer-scale polymer deformations are the tip radius, R_{tip}, polymer radius of gyration, R_g, Navier slip length, and tube diameter or distance between polymer entanglements, ξ_0.[13] In AFM nanoindentation of high M_W polymer films, $R_{tip} > \xi_0$ and $R_{tip} \sim R_g$, suggesting that the viscous flow will be full slip at the polymer−tip interface.[13] However, polymer viscosity at this scale may be different from bulk viscosity due to molecular confinement in the thin polymer film.[14]

Several experiments of AFM nanoindentation have shown that the measured polymer response is different than would be expected in bulk polymer, for both isothermal[15−17] and nonisothermal[5] indentation conditions. For nonisothermal AFM nanoindentation, heat was applied only to the AFM tip while the polymer was initially at room temperature.[5] For isothermal AFM nanoindentation, the polymer and AFM tip were at identical temperature.[15−17] Isothermal indentations at room temperature found that within 5 nm of the polymer free surface the polymer modulus was 30% lower than that of the bulk.[16] Similar experiments also found anisotropy in the film mechanical properties.[17] Isothermal indentations above and below T_g found that the temperature dependence of the polymer mechanical properties was reduced compared to the bulk.[15] Possible explanations for the observed behaviors included free surface mobility reducing modulus[16] and enhancing wetting,[15] strain-

* Corresponding author: Ph (217) 244-3864; Fax (217) 244- 6534; e-mail wpk@uiuc.edu.

10.1021/ma0704358 CCC: $37.00
Published on Web 10/03/2007

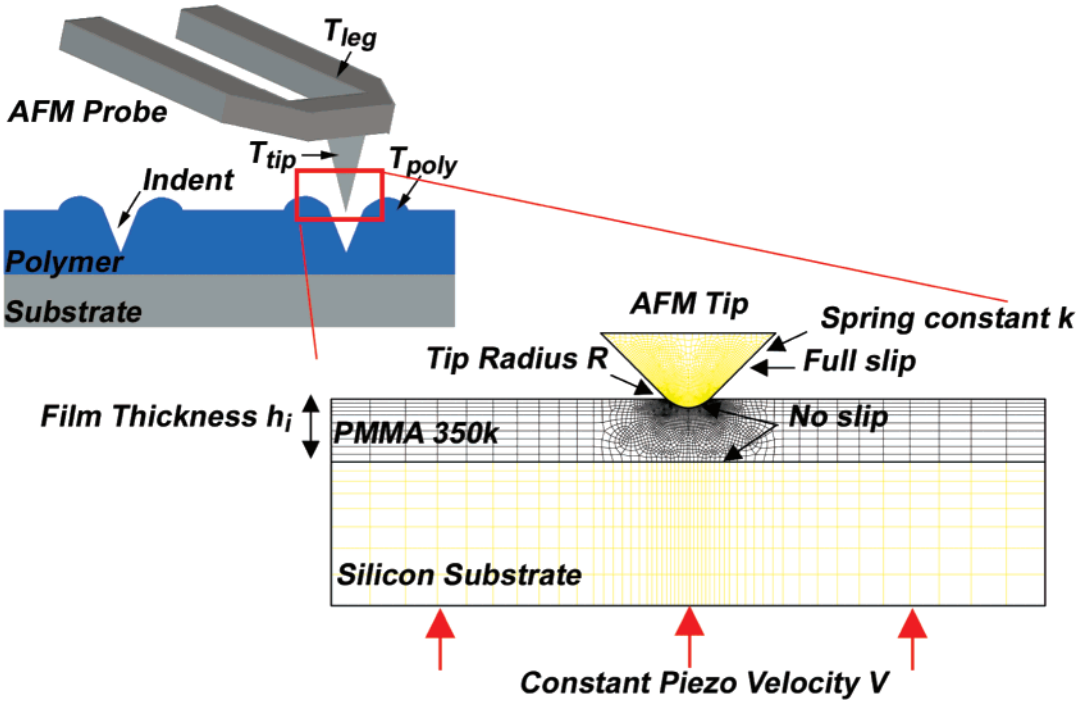

Figure 1. Atomic force microscope (AFM) nanoindentation. An AFM tip presses into a supported thin polymer layer where the probe leg temperature, tip temperature, and polymer temperature may have different values. The FEM model shows geometry and boundary conditions for isothermal nanoindentation of 350K M_W PMMA at constant piezovelocity. To aid convergence, the tip initially in contact with the polymer does not slip.

induced structuring during sample preparation,[17] and high localized pressure.[15] Nonisothermal nanoindentation formation showed high-frequency polymer viscosity that was independent of chain length, with the requirement that the heater temperature be well above bulk T_g in order to form indents.[5] Simulations accounting for phonon scattering and contact resistance at the polymer−tip interface showed shear rate- and temperature-dependent viscous and elastic polymer response explained the observed behavior,[18] yet analytical models showed instantaneous compressive heating could also explain the behavior.[19] Because of the complex polymer mechanical response, heat transfer characteristics, and observed deviation from bulk behavior, there is a lack of understanding of polymer deformation during polymer thin film nanoindentation.

This paper uses modified continuum simulations to investigate polymer flow during AFM nanoindentation, for both isothermal and nonisothermal conditions. The simulations examine a constant temperature sharp probe tip indenting a 35 nm film of high-M_W poly(methyl methacrylate) (PMMA). Isothermal simulations compare well with experimental results and highlight the importance of bulk shear-thinning material properties and slip at the polymer−tip interface. Nonisothermal simulations show the importance of high polymer−tip interface temperatures due to steep temperature and viscosity gradients within 50 nm of the polymer−tip interface.

Simulation Approach

The broad range of time scales and underlying structure of polymer melts, from angstrom level backbone to R_g of tens of nanometers, prohibits any one simulation method from capturing all physical processes.[20] An accurate model of AFM nanoindentation should capture the physics of highly entangled polymers of M_W near 500K on length scales 10−100 nm and time scales 1−100 ns. Molecular dynamics methods can track individual atoms but are generally limited to 100 monomer chains and 5 nm computational space with picosecond time steps.[20] Coarse-grained potentials can simulate non-Newtonian[20] and viscoelastic flow[21] with nanosecond time steps and microsecond processes[22] of polymers with $M_W > 100K$[23] by modeling 10−20 monomers as bonded blobs. In AFM nanoindentation, large penetration depths and temperature gradients can confine deformation zones to 5−10 nm, limiting coarse-grained solution methods to only 5−10 effective monomer blobs in the area of interest. Further, at present, coarse-grained methods are appropriate for a limited temperature range.[23] The three-dimensional, multiscale heat transfer and polymer deformation in AFM nanoindentation render it beyond reach of atomistic simulations.[24] This work uses continuum simulations with modified boundary conditions to model polymer melts in AFM nanoindentation, where the boundary conditions capture length scale-dependent slip.

The present simulations are performed using *GOMA*,[25] a finite element program specialized for analysis of complex polymer flows having a freely moving surface. *GOMA*, whose name derives from the Spanish word for "rubber", has been used for physical problems with length scales from 100 nm to 1 mm for processes such as deformable roll-coating and journal bearing lubrication,[26] micropen lithography,[27] and embossing imprint lithography.[28,29] *GOMA* provides two solution techniques to track the moving polymer interface: a front-tracking technique, the arbitrary Langrangian/Eulerian (ALE) method, and a front-capturing technique, the level set (LS) algorithm. ALE separates polymer motion from mesh motion, allowing large free boundary deformations.[30] LS tracks the liquid interface through a fixed mesh by following a function abstracted from the velocity field.[31,32] LS may require denser meshes than ALE to avoid mass loss and provide reliable convergence. In this paper, isothermal AFM nanoindentation simulations use ALE for fast simulation times while nonisothermal AFM nanoindentation simulations use LS to capture the large interfacial deformation at the polymer−tip interface. Both solution methods solve proper boundary conditions and governing equations of Navier−Stokes momentum and continuity:

$$\rho\left(\frac{\partial v}{\partial t} + v\cdot\nabla v\right) = -\nabla p + \frac{\eta}{2}\nabla\cdot(\nabla v + \nabla v^T) \quad (1)$$

$$\nabla\cdot v = 0 \quad (2)$$

where ρ is the liquid density, v liquid velocity, t time, p isotropic liquid pressure, and η liquid viscosity. Boundary conditions differ for isothermal and nonisothermal simulations. For nonisothermal AFM nanoindentation, heat transfer is also coupled into the solution:

$$\frac{\partial(\rho C_p T)}{\partial t} = -v\cdot\nabla(\rho C_p T) - \nabla\cdot q \quad (3)$$

where C_p is the heat capacity, T temperature, and q conduction heat flux.

In AFM nanoindentation, two effects govern motion of tip indentation in polymer: slip at the indenter−polymer interface due to size effects when $R_{tip} \sim R_g$,[13] and slip of polymer chains within the polymer. At high strain or shear rates, such as exist in AFM nanoindentation, bulk polymer chains disentangle, resulting in segments of polymer molecules that follow Rouse dynamics.[33−36] Constitutive models for a non-Newtonian stress tensor with adjusted boundary conditions can capture behavior of confined polymer melts. Since $R_{tip} > \xi_0$ and $R_{tip} \sim R_g$, the present simulations model a full-slip polymer−tip boundary. To capture rate-dependent polymer response, an inelastic Carreau shear-thinning material models the polymer. The Carreau material model captures reptation at low shear rates and Rouse dynamics at high shear rates by Newtonian viscosities. Although the inelastic Carreau model cannot properly predict normal stress ratios during polymer flow, the Carreau model can well approximate polymer behavior similar to more advanced viscoelastic models when deformation thinning dominates over normal stresses and relaxation.[37] By applying the Cox−Merz rule,[38] the Carreau model combines elastic and viscous effects to match measurements. Material data from[39] 200K M_W PMMA, with low stereotactic content and conventional mechanical properties, were fit to the Carreau model with high shear rate Rouse viscosity determined by

$$\eta_{Rouse} = \frac{\pi}{12}\left(\frac{\rho RT}{M_C}\right)\tau_e \quad (4)$$

where η_{Rouse} is the Rouse polymer viscosity in free space, R universal gas constant, T temperature, M_C critical molecular weight for high-M_W polymers, and τ_e polymer relaxation time denoting onset of tube constraint effects.[36] Equation 4 is based on $\eta_{Rouse}(M_C)$ and not $\eta_{Rouse}(M_W)$ as appropriate[35,36,40] since $\eta_{Rouse}(M_W)$ at high shear rates underestimates measurements of complex viscosity at similar shear rates.[39] Further, rheological measurements at high shear rates have shown the high shear rate Newtonian regime to be independent of M_W.[41] The temperature dependence of the polymer viscosity is accounted for by the Williams−Landel−Ferry (WLF) equation. The resulting Carreau−WLF viscosity model is

$$\eta = a_T[\eta_{Rouse} + (\eta_0 - \eta_{Rouse})(1 + (a_T\tau_d\,\dot{\gamma})^a)^{n-1/a}] \quad (5)$$

where η_0 is the zero shear polymer viscosity, τ_d terminal relaxation or disengagement time, $\dot{\gamma}$ shear rate, a fitting parameter, and n shear-thinning exponent. The WLF shift factor a_T is

$$\log a_T = \frac{C_1(T - T_{ref})}{C_2 + T - T_{ref}} \quad (6)$$

where C_1 and C_2 are material constants and T_{ref} is the reference temperature. At the reference temperature 190 °C for 200K M_W PMMA, η_0 is 4.7×10^6 Pa·s, τ_d is 25 s, a is 1, n is 0.17, C_1 is 8.6, and C_2 is 180 °C. The viscosity of each element in the simulation is locally determined, dependent on shear rate and temperature. The Carreau model fits PMMA of various M_W by scaling η_0 and τ_d by $(M_W/200K)^{3.4}$. The Carreau model represents a range of polymer deformation mechanisms: zero shear viscosity describes the viscous flow region, power law shear-thinning describes the rubbery plateau region, and high shear rate Rouse viscosity describes the glass−rubber transition region.

The continuum simulations are able to reasonably account for the AFM nanoindentation process because high shear rates govern the polymer deformation. The polymer properties affected by high shear rate deformation are not dependent on full chain length mechanics (∼25−50 nm) but instead operate over a much shorter distance. The simulations account for short-range, high shear rate polymer mobility modes with the power law and Rouse viscosity components of the Carreau shear model. In this regime, continuum mechanics works well. The influence of tacticity on measured and simulated mechanical properties is also diminished in the high shear rate regime since M_C does not appreciably vary with tacticity.[39] While it can be expected that the temperature-dependent mechanical properties of the thin film PMMA are different from bulk, to the best of the authors' knowledge, there exists no well-accepted quantitative measurement of PMMA mechanical modulus at the nanometer scale over a range of temperatures and times that could inform the predictions of the present work. Thus, the present simulations use bulk polymer properties and estimate the likely difference between bulk property values and thin film values as modeling error.

Results and Discussion

The present simulations investigated both isothermal and nonisothermal AFM nanoindentation into a polymer thin film. In the isothermal case, both tip and substrate were heated. In the nonisothermal case, only the AFM tip was heated.

I. Isothermal AFM Nanoindentation. The isothermal simulations modeled polymer flow in a 35 nm film of 350K M_W PMMA supported by a silicon substrate. The substrate approached a silicon AFM tip of radius 20 nm and spring constant 40 N/m at constant velocity 160 nm/s. A no-slip polymer−substrate boundary condition modeled the interface between the polymer film and the underlying silicon.[42−44] A full-slip condition modeled the polymer−tip interface. For swift convergence, the AFM tip was initially embedded 5 nm in the polymer with a no-slip condition. Assuming the AFM tip represents a sphere in Stokes flow, the small contact area of no-slip introduces an error <10% compared to full-slip Stokes flow.[45] The goal of the isothermal simulations was to simulate a previously measured situation.[15]

Figure 1 shows the model and boundary conditions for isothermal AFM nanoindentation. The simulations predicted indentations governed by shear-thinning polymer behavior at temperatures from 115 to 135 °C, where T_g is 120 °C.[39] The indenting AFM tip produced a distribution of shear rates in the polymer, localized near the tip. Figure 2a shows viscosity contours in the polymer during indentation where the viscosity was normalized by the Rouse viscosity at the indicated

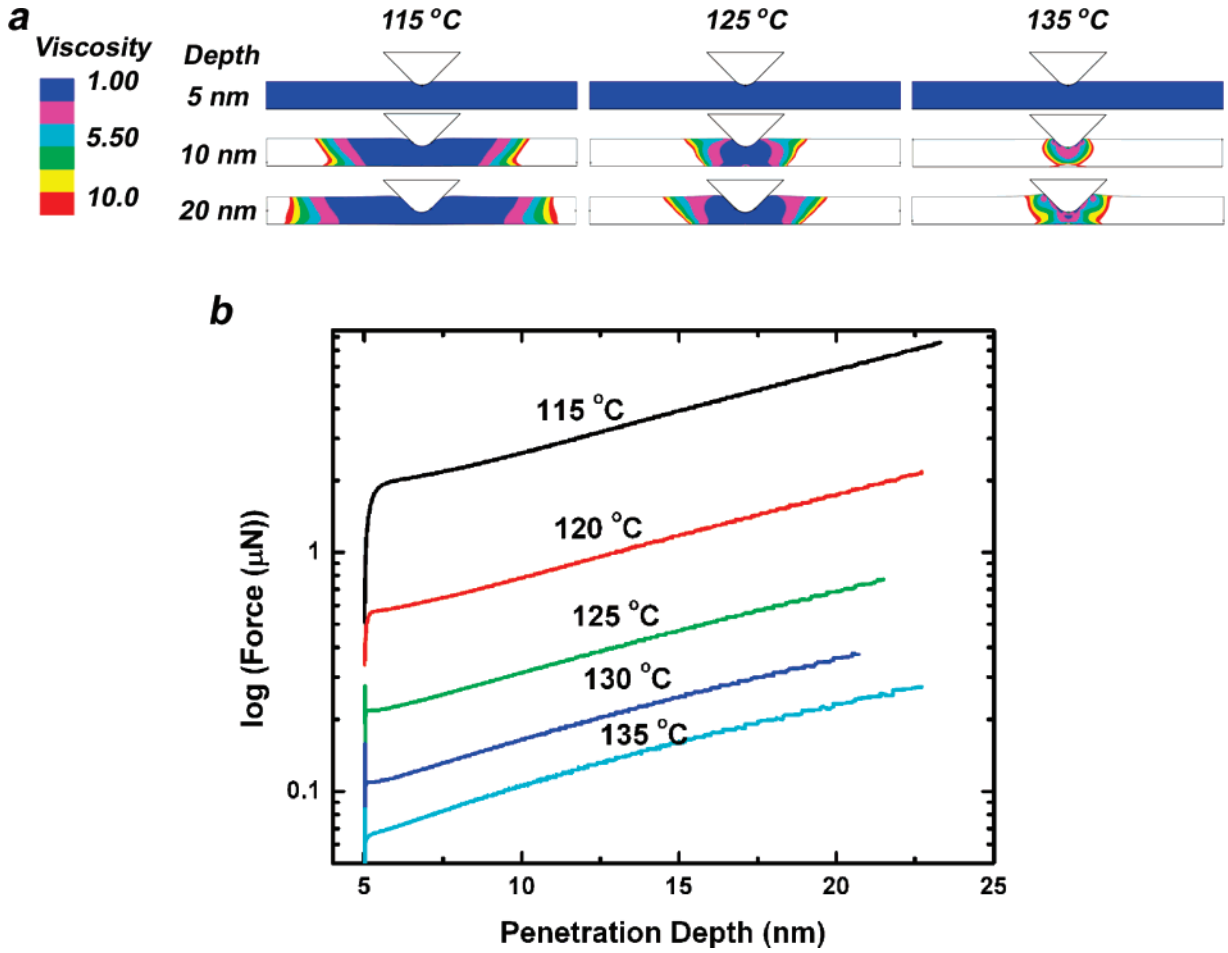

Figure 2. Deformation profiles and loading curves for isothermal AFM nanoindentation. (a) Indentation profiles showing viscosity contours for isothermal indentation at different temperatures. Dimensionless viscosity of 1.00 corresponds to polymer Rouse viscosity at indicated temperature. Shear rates increase at deeper penetration depth. (b) Semilog loading curves under isothermal conditions. The loading curves at different temperatures cannot be superimposed by appropriate WLF scaling due to the nonlinear shear-thinning polymer response. The simulation material model does not properly account for deformation processes below T_g where the simulation predicts material deformation at a constant Newtonian Rouse viscosity.

temperature. The shear rates experienced by the polymer were similar for all temperatures. However, as temperature increased, the polymer response changed from a nearly constant Rouse viscosity response to a power-law viscosity response. At 115 °C, the polymer viscosity contours were nearly constant within 100 nm of the tip. At 135 °C, the polymer viscosity contours varied by over an order of magnitude within 25 nm of the tip. The local variation in polymer viscosity only occurred at high temperatures as the Carreau model predicted a shear-rate-independent Rouse viscosity at low temperatures but a shear-rate-dependent power law viscosity at high temperatures. The polymer shear-thinning induced a mechanical response that was different from a constant viscosity response.

Figure 2b shows the force on the tip during indentations where the tip velocity was constant. The jump in force at initial penetration depth is a simulation artifact resulting from changes in material models required to initiate simulation convergence. The large variation of polymer properties with shear rate in Carreau material models of 350K M_W PMMA resulted in difficulty obtaining simulation convergence at the start of indentation. Thus, simulations first modeled 35K M_W for short time steps and used the converged solution field to start simulations modeling 70K M_W. This process was repeated until the simulations converged modeling 350K M_W PMMA.

The simulated force vs penetration curves shown in Figure 2b suggest that force scales exponentially with penetration depth for constant viscosity fluids but not for power-law fluids. At 130 and 135 °C, where the polymer was characterized by a power-law viscosity, simulated force vs penetration plots showed significant curvature on semilog axes, indicating the force did not scale exponentially with penetration depth. At low temperatures near T_g, where the polymer was characterized by a constant Rouse viscosity, force scaled exponentially with penetration depth, although the analytical solution of force vs penetration is much more complicated.[46] The exponential scaling of force with penetration depth at low temperatures is not necessarily valid for all polymers since the simulated material model cannot capture shear-thinning behavior at high shear rates beyond the constant Rouse viscosity zone. However, the present simulations suggest that force scales exponentially with penetration depth during AFM nanoindentation at sufficiently high temperatures or low shear rates where the polymer viscosity can be represented with a high degree of accuracy by a constant-viscosity Newtonian fluid. The force vs penetration curves in Figure 2b cannot be vertically collapsed to a universal loading curve by a simple WLF scaling since the low-temperature curves are governed by a constant Rouse viscosity and the high-temperature curves are governed by a power-law viscosity.

Simulated force−distance curves matched well with experimental force−distance curves over a range of temperatures. Figure 3a shows force−distance curves predicted by simulation and measured force−distance curves at two temperatures, where the measurements are from previously published results.[15] At temperatures just above T_g, 122 °C simulation closely matched

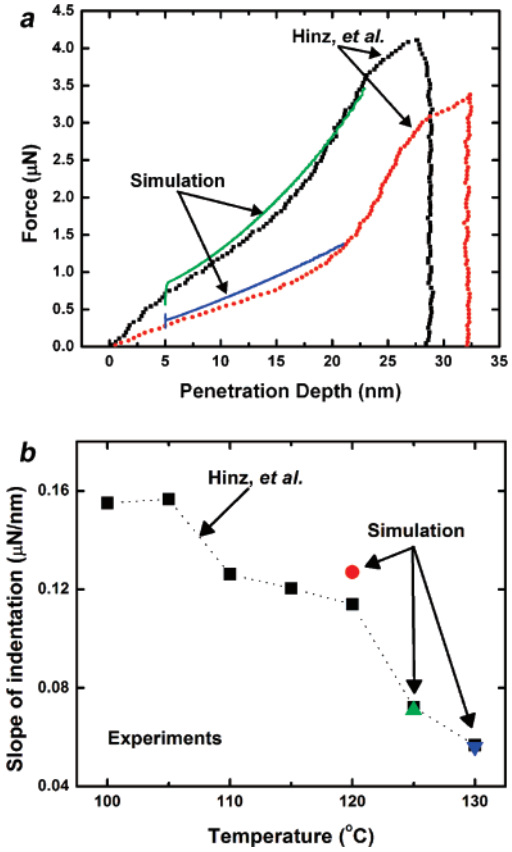

Figure 3. Polymer response during isothermal nanoindentation described by bulk high shear rate behavior. (a) Force vs depth indentation curves show simulation just above T_g matches glassy polymer indent and simulation at 130 °C matches experiment at 130 °C. (b) Simulation initial slope of indentation also closely matches experimental data over the same temperature range. At higher temperatures, the slope of indentation approaches the cantilever spring constant. The data are from Hinz and co-workers.[15]

glassy 100 °C measurements. The unexpected agreement of Carreau simulation to glassy data may have been due to simulated properties different from experimental parameters. In particular, the experiments[15] could have been influenced by a polydisperse sample with broad glass transition and rapid quenching during film preparation, which could cause experimentally observed enhanced mechanical compliance near T_g. Simulated and measured force−distance curves matched well at 130 °C while simulation indentation slope at 122, 125, and 130 °C closely corresponded to measured indentation slope at 120, 125, and 130 °C, respectively.[15] For an elastic contact, the initial slope of indentation can determine the polymer modulus.[47] The agreement of Carreau simulation slope of indentation and measurements, shown in Figure 3b, suggests the dominance of viscoelastic shear-thinning over elastic polymer properties during isothermal indentation near T_g. The slope of indentation at $T > 130$ °C approached 40 N/m, limiting measurements and simulation of polymer mechanical properties to $T < 135$ °C due to compliance coupling of the polymer modulus to the cantilever stiffness.

Comparisons between model and experiment were limited to penetration depths <20 nm due to simulation constraints of mesh deformation at large strains. At tip penetration depths >20 nm, the simulation would underestimate polymer force response, as measurements showed a sharp increase in force vs displacement. This stiffening could be due to the shape of the tip, high shear rate elastic stiffening during squeeze flow,[48] or attractive surface interactions between polymer and substrate.[8,42,43] At tip penetration depths <20 nm, potential sources of simulation error could arise from contact conditions. If the polymer−tip interface or polymer−substrate interface were no-slip, the current simulations underestimated the force response by a factor of 1.5[45] or 30%,[46] respectively. The no-slip interfaces would require higher simulation temperatures to match experimental results of ref 15. Any errors introduced by contact interaction will be constant across the temperature range, limiting accuracy in fitting proper simulation and measurement temperature but not the precision of the Carreau WLF material behavior.

II. Nonisothermal AFM Nanoindentation. Figure 4a shows the FEM model and boundary conditions for the nonisothermal simulations. The AFM tip is heated such that there was an externally fixed polymer−tip interface temperature, while the surrounding polymer was initially at room temperature. The simulations do not solve the complex subcontinuum heat transfer through the AFM probe tip to the polymer and instead fix the temperature at the tip−polymer interface. The conditions were chosen to represent thermomechanical data storage.[5] The polymer was a 35 nm thick 75K M_W PMMA film with isotropic bulk thermal conductivity 0.18 W/(m K) and heat capacity 1450 J/(K kg). Beneath the polymer was 80 nm cross-linked epoxy with identical thermal properties as the polymer and a silicon substrate of bulk thermal conductivity 150 W/(m K) and heat capacity 700 J/(K kg). Polymer bilayer and silicon substrate boundaries were at 25 °C. The LS simulations required modeling of a small air region with density and viscosity 2 orders of magnitude less than the polymer layer, which are slightly less than bulk values. The air boundary was modeled as adiabatic since the cantilever−substrate air gap equilibrates in ~100 ns, and it is known that the heat transfer across this interface is not important for the indent formation.[18] The tip loading force was 30 nN, the radius 30 nm, and the loading force approximately constant due to the small displacements employed. The tip was also modeled with a large inertial mass equivalent to the effective mass of a typical cantilever beam, thus providing a lower limit to indentation speed based on the cantilever mechanical time constant.[18] The simulations assumed a no-slip boundary condition at the PMMA−epoxy interface and a full-slip condition at the polymer−tip interface.

Predictions showed polymer deformation localized near the AFM tip. Figure 4b shows deformation profiles for polymer−tip interface temperature T_{int} 250 °C. The tip locally heated the polymer, creating a temperature gradient from the tip temperature to 25 °C within 50 nm from the polymer−tip interface. Over this range, the temperature-dependent complex viscosity varied by several orders of magnitude, resulting in localized deformation of high-temperature polymer within 5−10 nm of the tip. The simulated heat-effected zone with radius ~50 nm from the AFM tip defines the minimum spacing between indentations for data storage applications. Experiments have shown that forming a second data bit (indentation crater) within a distance <40 nm from a previously formed data bit modifies the residual indent of the previously formed data bit. This feature has been exploited to erase data bits by dense indentations.[5]

Polymer−tip interface temperatures >200 °C were required for significant penetration depth in 10 μs for tip pressures <1 GPa, which corresponds with general experimental observations.[5] Figure 5 shows the penetration depth after 10 μs for AFM tip radius 20 nm at 30, 100, and 500 nN from T_{int} 175−300 °C. The temperature-dependent penetration curves cannot be superimposed by appropriate WLF scaling due to the nonlinear shear-thinning polymer response. For a given polymer−tip interface temperature, increasing load increased penetration depth. However, at $T_{int} < 200$ °C, indentation rates were <0.5

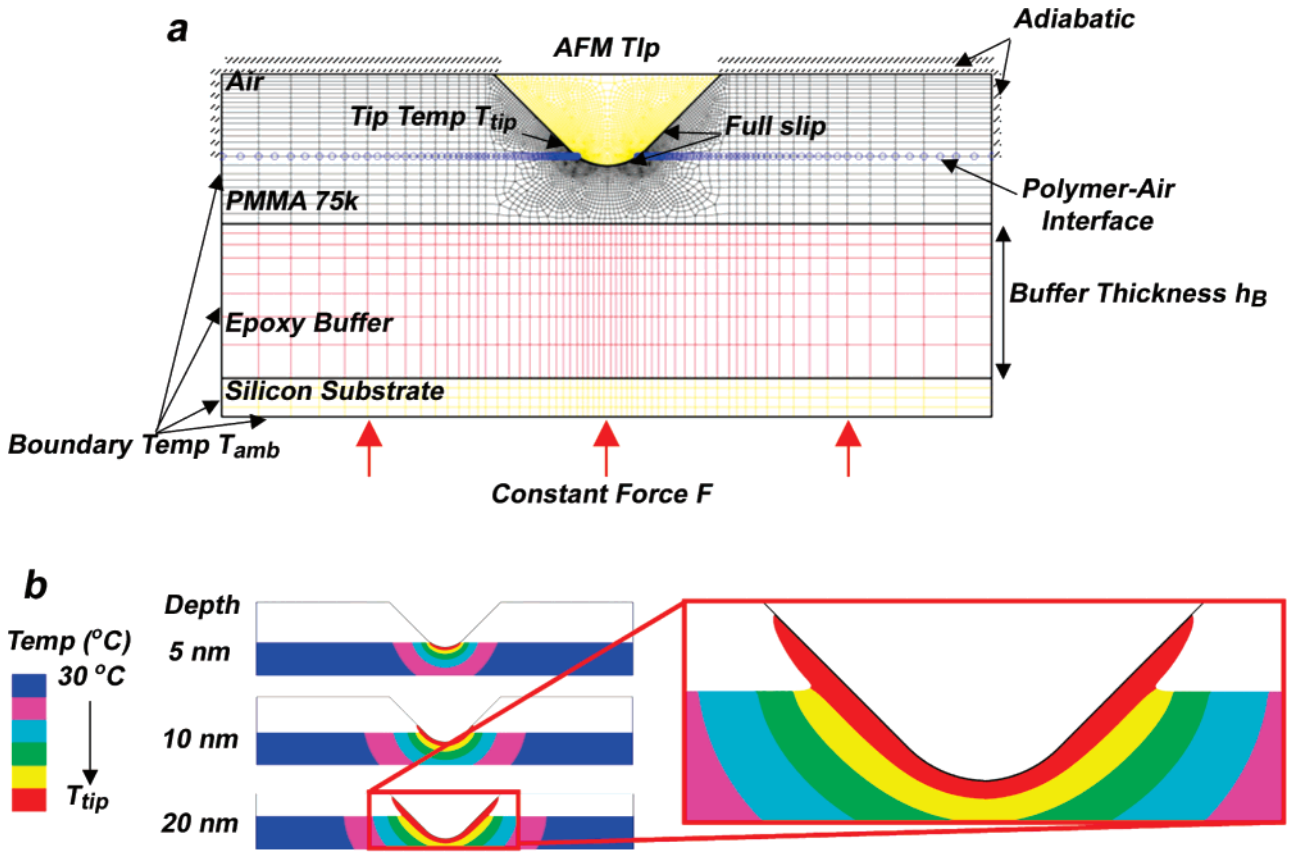

Figure 4. Modified continuum simulations guide predictions of nonisothermal nanoindentation. (a) Nonisothermal nanoindentation of AFM tip with full slip and constant temperature tip−fluid interface into ambient polymer at constant force. (b) Indentation profiles showing temperature contours in 75K M_W PMMA polymer for tip−polymer interface temperature $T_{int} = 250$ °C and ambient temperature $T_{amb} = 30$ °C. The steep spatial gradient of the temperature shift factor results in highly localized polymer deformation resembling lubrication. Relaxed shift factor and increased segmental cooperativity lengths in confined geometries would broaden deformation.

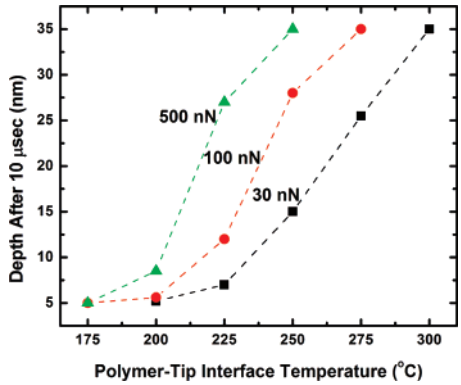

Figure 5. Simulation predictions of the required polymer−tip interface temperature for an AFM tip of radius 30 nm to form a data bit in 10 μs. Forces >500 nN are required to form 10 nm indentations in 10 μs at $T_g + 80$ °C. Polymer−tip interface temperatures >200 °C are required for significant penetration depth in 10 μs for tip pressures <1 GPa.

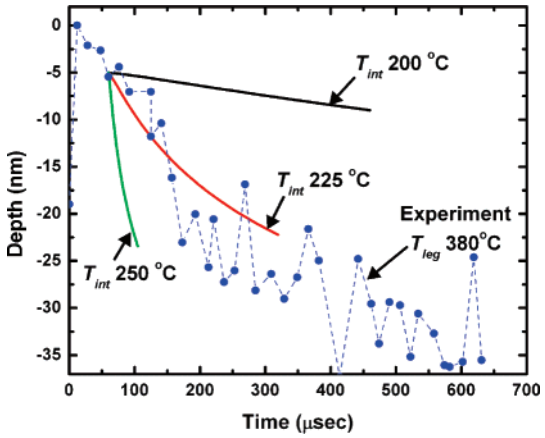

Figure 6. Measurements (dotted lines) and simulations (solid lines) of nonisothermal AFM nanoindentation for nanoprobe data storage. Simulation of 75K M_W PMMA for tip−polymer interface temperature $T_{int} \sim 240$ °C matches experiment for indentation into 600K M_W PMMA at cantilever leg temperature of 380 °C. Heat transfer modeling predicts $T_{int} \sim 250$ °C[18] for similar conditions. Tip radius is 30 nm.

nm/s regardless of load. The steep temperature and viscosity gradient within 50 nm from the polymer−tip interface resulted in insufficient polymer softening to form deep indentations when $T_{int} < T_g + 80$ °C.

Predictions compare well with measurement, which is reported elsewhere in detail[5] and only summarized here. For the experiments, a heated AFM cantilever with tip radius 30 nm indented a 35 nm film of 600K M_W PMMA supported by 80 nm SU-8 epoxy on a silicon substrate. A 28 nN load pressed the tip against the polymer surface initially at room temperature with negligible penetration. The cantilever was heated to 380 °C, transferring sufficient heat to the AFM tip to allow the tip to indent the polymer. The AFM tip motion was measured via laser beam deflection.

Figure 6 shows the data for indentations in 600K M_W PMMA at cantilever heater temperature 380 °C and simulation predictions for indentation into 75K M_W PMMA at T_{int} from 200 to 250 °C. Simulations at T_{int} 225 and 250 °C suggest $T_{int} \sim 240$ °C predicts measured material response, in agreement with heat transfer modeling that predicts $T_{int} \sim 250$ °C for cantilever leg temperatures near 380 °C at 30 nN load.[18] A temperature drop

along the tip of about 100 °C is consistent with simulations[18] and measurements[49] of subcontinuum heat flow in the tip, where thermal resistance in the tip and thermal contact resistance likely cause the low polymer−tip interface temperature corresponding to the high cantilever leg temperature.

Simulations were limited to $M_W < 75K$ due to numerical instabilities of the viscosity gradient in the locally deforming polymer. Modeling $M_W > 75K$ would increase T_{int} and produce a result that more closely matches measurements, though the high shear rates and strongly shear-thinning polymer would likely only increase T_{int} by about 25 °C. Hydrostatic pressures due to tip load could also increase simulated T_{int}; however, a 30 nN load would only increase T_g by at most 2 °C.[50]

Overall, the simulations suggest that logarithmic viscosity gradients caused by temperature gradients in the polymer govern the bit writing process. However, the simulations predict most of the polymer flow in a region of thickness 5−10 nm while measured AFM traces after indentation show a broader deformation profile.[5] The shape of the free surface should not greatly influence the simulation mechanical response as viscoelastic effects dominate capillary effects during the indentation time scale. The present continuum mechanics simulations are able to effectively capture the polymer response in such small deformation areas due to the importance of short-range polymer mobility modes in the AFM nanoindentation process represented by the high shear rate power-law viscosity and Rouse viscosity. The high shear rate polymer mobility modes operate over a distance much shorter than full chain length polymer mechanics. Several physical phenomena not accounted for in simulations would broaden the simulated free surface deformation. Enhanced cooperativity of polymer mobility modes,[8,51] reduced temperature dependence of viscosity,[10] and anisotropic thermal conductivity[52] have been measured in thin polymer films. These effects would result in larger volumes of similar viscosity material adjacent to the tip and broaden the polymer deformation.

Conclusions

This paper uses continuum simulations of polymer flow with modified boundary conditions to predict nanometer-scale polymer deformation. The continuum simulations accurately model subcontinuum polymer mechanical response during AFM nanoindentation from initial film thickness $\sim 2R_g$ to residual film thickness below R_g but highlight the need for nanoscale material property measurements to accurately model deformation shape. High-M_W polymer films during isothermal AFM nanoindentation follow shear-thinning bulk material behavior with a full-slip polymer−tip interface, in agreement with predictions of ref 13. Nonisothermal AFM nanoindentation simulations show logarithmic viscosity gradients caused by temperature gradients in the polymer govern the bit writing process. The continuum simulations allow for optimization of nanoprobe data storage and high-resolution NIL based on bulk viscoelastic material properties and extend continuum descriptions of polymer mechanics to length scales below R_g.

Acknowledgment. The authors thank Martin Hinz for generously sharing data and Chris Brotherton, Rekha Rao, and Tom Baer for simulation assistance. The authors acknowledge funding support from Sandia MESA Institute, an NSF CAREER Award CBET-0238888, NSF Award CMS-0527275, the Office of Naval Research, and a PECASE award from the Department of Energy.

References and Notes

(1) Hua, F.; Sun, Y.; Gaur, A.; Meitl, M. A.; Bilhaut, L.; Rotkina, L.; Wang, J.; Geil, P.; Shim, M.; Rogers, J. A. Polymer Imprint Lithography with Molecular-Scale Resolution. *Nano Lett.* **2004**, *4*, 2467−2471.
(2) Xu, Q.; Mayers, B. T.; Lahav, M.; Vezenov, D. V.; Whitesides, G. M.; Approaching Zero: Using Fractured Crystals in Metrology for Replica Molding. *J. Am. Chem. Soc.* **2005**, *127*, 854−855.
(3) Chou, S. Y.; Krauss, P. R.; Renstrom, P. J. Imprint of sub-25 nm vias and trenches in polymers. *Appl. Phys. Lett.* **1995**, *67*, 3114−3116.
(4) Khang, D.; Lee, H. Wafer-scale sub-micron lithography. *Appl. Phys. Lett.* **1999**, *75*, 2599−2601.
(5) Vettiger, P.; Cross, G.; Despont, M.; Drechsler, U.; During, U.; Gotsmann, B.; Haberle, W.; Lantz, M. A.; Rothuizen, H. E.; Stutz, R.; Binning, G. K. The "Millipede"-Nanotechnology Entering Data Storage. *IEEE Trans. Nanotechnol.* **2002**, *1*, 39−55.
(6) Granick, S.; Kumar, S.; Arnis, E.; Antonietti, M.; Balazs, A.; Chakraborty, A.; Grest, G.; Hawker, C.; Janmey, P.; Kramer, E.; Nuzzo, R.; Russell, T.; Safinya, C. Macromolecules at surfaces: Research, challenges and opportunities from tribology to biology. *J. Polym. Sci., Part B: Polym. Phys.* **2003**, *41*, 2755−2793.
(7) Alcoutlabi, M.; McKenna, G. B. Effects, of confinement on material behaviour at the nanometre size scale. *J. Phys.: Condens. Matter* **2005**, *17*, R461−R524.
(8) Ellison, C. J.; Torkelson, J. M. The distribution of glass-transition temperatures in nanoscopically confined glass formers. *Nat. Mater.* **2003**, *2*, 695−700.
(9) Sills, S.; Overney, R. M.; Chau, W.; Lee, V. Y.; Miller, R. D.; Frommer, J. Interfacial glass transition profiles in ultrathin, spin cast polymer films. *J. Chem. Phys.* **2004**, *120*, 5334−5338.
(10) Li, C.; Koga, T.; Li, C.; Jiang, J.; Sharma, S.; Narayanan, S.; Lurio, L. B.; Hu, X.; Jiao, X.; Sinha, S. K.; Billet, S.; Sosnowik, D.; Kim, H.; Sokolov, J. C.; Rafailovich, M. H. Viscosity Measurements of Very Thin Polymer Films. *Macromolecules* **2005**, *38*, 5144−5151.
(11) Frank, B.; Gast, A. P.; Russell, T.; Brown, H. R.; Hawker, C. Polymer Mobility in Thin Films. *Macromolecules* **1996**, *29*, 6531−6534.
(12) Mamin, H. J.; Rugar, D. Thermomechanical writing with an atomic force microscope tip. *Appl. Phys. Lett.* **1992**, *61*, 1003−1005.
(13) Brochard, F.; de Gennes, P. G. Viscosity at small scales in polymer melts. *Eur. Phys. J. E* **2000**, *1*, 93−97.
(14) Keddie, J. L.; Jones, R. A. L.; Cory, R. A. Size-dependent depression of the glass-transition temperature in polymer-films. *Europhys. Lett.* **1994**, *27*, 59−64.
(15) Hinz, M.; Kleiner, A.; Hild, S.; Marti, O.; During, U.; Gotsmann, B.; Drechsler, U.; Albrecht, T. R.; Vettiger, P. Temperature dependent nano indentation of thin polymer films with the scanning force microscope. *Eur. Polym. J.* **2004**, *40*, 957−964.
(16) Miyake, K.; Satomi, N.; Sasaki, S. Elastic modulus of polystyrene film from near surface to bulk measured by nanoindentation using atomic force microscopy. *Appl. Phys. Lett.* **2006**, *89*, 031925.
(17) Sills, S.; Overney, R. M.; Gotsmann, B.; Frommer, J. Strain shielding and confined plasticity in thin polymer films: Impacts on thermomechanical data storage. *Tribol. Lett.* **2005**, *19*, 9−15.
(18) King, W. P. Thermomechanical Formation of Polymer Nanostructures. Ph.D. Stanford University, Palo Alto, CA, 2002.
(19) Mackay, M. E. A Simple Model for the Millipede Write Technique. *IEEE Trans. Nanotechnol.* **2005**, *4*, 641−644.
(20) Glotzer, S. C.; Paul, W.; Molecular and Mesoscale Simulation Methods for Polymer Materials. *Annu. Rev. Mater. Res.* **2002**, *32*, 401−436.
(21) ten Bosch, B. I. M. On an extension of Dissipative Particle Dynamics for viscoelastic flow modelling. *J. Non-Newtonian Fluid Mech.* **1999**, *83*, 231−248.
(22) Koumoutsakos, P.; Multiscale Flow Simulations Using Particles. *Annu. Rev. Fluid Mech.* **2005**, *37*, 457−487.
(23) Ashbaugh, H. S.; Patel, H. A.; Kumar, S.; Garde, S. Mesoscale model of polymer melt structure: Self-consistent mapping of molecular correlations to coarse-grained potentials. *J. Chem. Phys.* **2005**, *122*, 104908-1−104908-5.
(24) Cahill, D. G.; Ford, W. K.; Goodson, K. E.; Mahan, G. D.; Majumdar, A.; Maris, H. J.; Merlin, R.; Phillpot, S. R. Nanoscale thermal transport. *J. Appl. Phys.* **2003**, *93*, 793−818.
(25) Schunk, P. R.; Sackinger, P. A.; Rao, R. R.; Chen, K. S.; Baer, T. A.; Labreche, D. A.; Sun, A. C.; Hopkins, M. M.; Subia, S. R.; Moffat, H. K.; Secor, R. B.; Roach, R. A.; Wilkes, E. D.; Noble, D. R.; Hopkins, P. L.; Notz, P. K.; Goma 4.0- A Full-Newton Finite Element Program for Free and Moving Boundary Problems with Coupled Fluid/Solid Momentum, Energy, Mass, and Chemical Species Transport: User's Guide. Sandia National Laboratories Technical Report SAND2002-3204, 2002.
(26) Stay, M. S.; Barocas, V. H.; Couple lubrication and Stokes flow finite elements. *Int. J. Numer. Methods Fluids* **2003**, *43*, 129−146.

(27) Fan, H. Y.; Lu, Y.; Stump, A.; Reed, S. T.; Baer, T. A.; Schunk, P. R.; Perez-Luna, V.; Lopez, G. P.; Brinker, C. J.; Rapid prototyping of patterned functional nanostructures. *Lett. Nature* **2000**, *405*, 56−60.
(28) Rowland, H. D.; King, W. P.; Sun, A. C.; Schunk, P. R.; Impact, of polymer film thickness and cavity size on polymer flow during embossing: toward process design rules for nanoimprint lithography. *J. Micromech. Microeng.* **2005**, *15*, 2414−2425.
(29) Rowland, H. D.; King, W. P.; Sun, A. C.; Schunk, P. R.; Simulations, of nonuniform embossing: The effect of asymmetric neighbor cavities on polymer flow during nanoimprint lithography. *J. Vac. Sci. Technol., B* **2005**, *23*, 2958−2962.
(30) Sackinger, P. A.; Schunk, P. R.; Rao, R. R. A Newton-Raphson Pseudo-Solid Domain Mapping Technique for Free and Moving Boundary Problems: A Finite Element Implementation. *J. Comput. Phys.* **1996**, *125*, 83−103.
(31) Sethian, J. A. *Level Set Methods and Fast Marching Methods;* Cambridge University Press: New York, 1999.
(32) Baer, T. A.; Noble, D. R.; Rao, R. R.; Grillet, A. M. In *A Level Set Approach to 3D Mold Filling of Newtonian Fluids*; ASME Symposium on Flows in Manufacturing Processes, Honolulu, HI, July 6−10, 2003.
(33) Granick, S.; Hu, H.-W.; Carson, G. A.; Nanorheology, of Confined, Polymer, Melts. 2. Nonlinear Shear Response at Strongly Adsorbing Surfaces. *Langmuir* **1994**, *10*, 3867−3873.
(34) Awati, K. M.; Park, Y.; Weisser, E.; Mackay, M. E. Wall, slip and shear stresses of polymer melts at high shear rates without pressure and viscous heating effects. *J. Non-Newtonian Fluid Mech.* **2000**, *89*, 117−131.
(35) Tsenoglou, C. Non-Newtonian Rheology of Entangled Polymer Solution and Melts. *Macromolecules* **2001**, *34*, 2148−2155.
(36) Doi, M.; Edwards, S. F. *The Theory of Polymer Dynamics;* Oxford University Press: Oxford, 1999; Vol. 73.
(37) Wapperom, P.; Keunings, R. Simulation of linear polymer melts in transient complex flow. *J. Non-Newtonian Fluid Mech.* **2000**, *95*, 67−83.
(38) Cox, W. P.; Merz, E. H.; Correlation of Dynamic and Steady Flow Viscosities. *J. Polym. Sci.* **1958**, *28*, 619−622.
(39) Fuchs, K.; Friedrich, C.; Weese, J. Viscoelastic Properties of Narrow-Distribution Poly(methyl methacrylates). *Macromolecules* **1996**, *29*, 5893−5901.
(40) Graessley, W. W. Some Phenomenological Consequences of the Doi-Edwards Theory of Viscoelasticity. *J. Polym. Sci., Polym. Phys. Ed.* **1980**, *18*, 27−34.
(41) Hieber, C. A.; Chiang, H. H. Some correlations involving the shear viscosity of polystyrene melts. *Rheol. Acta* **1989**, *28*, 321−332.
(42) Priestley, R. D.; Broadbelt, L. J.; Torkelson, J. M. Physical Aging of Ultrathin Polymer Films above and below the Bulk Glass Transition Temperature: Effects of Attractive vs Neutral Polymer-Substrate Interactions Measured by Fluorescence. *Macromolecules* **2005**, *38*, 654−657.
(43) Fryer, D. S.; Nealey, P. F.; de Pablo, J. J. Thermal Probe Measurements of the Glass Transition Temperature for Ultrathin Polymer Films as a Function of Thickness. *Macromolecules* **2000**, *33*, 6439−6447.
(44) Frank, C. W.; Rao, V.; Despotopoulou, M. M.; Pease, R. F. W.; Hinsberg, W. D.; Miller, R. D.; Rabolt, J. F. Structure in Thin and Ultrathin Spin-Cast Polymer Films. *Science* **1996**, *273*, 912−915.
(45) Panton, R. L. *Incompressible Flow*, 2nd ed.; John Wiley & Sons: New York, 1996; p 837.
(46) Brenner, H. The slow motion of a sphere through a viscous fluid towards a plane surface. *Chem. Eng. Sci.* **1961**, *16*, 242−251.
(47) Capella, B.; Dietler, G. Force-distance curves by atomic force microscopy. *Surf. Sci. Rep.* **1999**, *34*, 1−104.
(48) Phan-Thien, N.; Dudek, J.; Boger, D. V.; Tirtaatmadja, V.; Squeeze Film Flow of Ideal Elastic Liquids. *J. Non-Newtonian Fluid Mech.* **1985**, *18*, 227−254.
(49) Nelson, B. A.; King, W. P. Measuring material softening with nanoscale spatial resolution using heated silicon probes. *Rev. Sci. Instrum.* **2007**, *78*, 023702.
(50) Stevens, J. R.; Coakley, R. W.; Chau, K. W.; Hunt, J. L. The pressure variation of the glass transition temperature in atactic polystyrene. *J. Chem. Phys.* **1986**, *84*, 1006−1014.
(51) Priestley, R. D.; Ellison, C. J.; Broadbelt, L. J.; Torkelson, J. M.; Structural Relaxation of Polymer Glasses at Surfaces, Interfaces, and In Between. *Science* **2005**, *309*, 456−459.
(52) Kurabayashi, K.; Asheghi, M.; Touzelbaev, M.; Goodson, K. E. Measurement of the thermal conductivity anisotropy in polyimide films. *J. Microelectromech. Syst.* **1999**, *8*, 180−191.

MA0704358